Ecological Indicators 178 (2025) 114046

Contents lists available at ScienceDirect

Ecological Indicators

journal homepage: www.elsevier.com/locate/ecolind

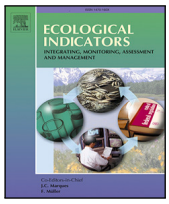

Original articles

Computing maps of forest structural diversity: Aggregate late

Tuomas Rajala [a],*, Annika Kangas [b], Mari Myllymäki [a]

[a] Natural Resources Institute Finland (Luke), Latokartanonkaari 9, FI-00791 Helsinki, Finland
[b] Natural Resources Institute Finland (Luke), Yliopistokatu 6, FI-80100 Joensuu, Finland

ARTICLE INFO

Keywords:
Biodiversity
Forest structure
Gini index
Local K function
Spatial point pattern
Spatial structure

ABSTRACT

Local forest biodiversity hotspots are small areas within a landscape or a single stand, characterised by a high variability in e.g. species composition, size distribution or spatial pattern, in comparison to the surrounding areas. Their identification is important, e.g. for planning routes of harvesters, for selecting retention tree groups from the cutting area, and for selecting set-aside areas at landscape level. Traditional optical remote sensing enables prediction of forest attributes at large areas, but is typically restricted to a fixed spatial resolution. The fixed resolution is problematic especially for diversity indices as it contradicts the ecological meaning of local diversity which varies as a function of scale. While traditionally diversity predictions were produced with area-based approaches, combining 3D point-cloud-data-based single tree detection with field data enables the production of tree-level data, creating new opportunities for forest structure quantification. Particularly, at the single-tree level the ecological scale can be separated from the technical resolution. We demonstrate the importance of distinguishing scales when producing forest diversity maps. Furthermore, local diversity indices are typically computed at systematically or randomly selected locations in the landscape. We present new, alternative indices, defined through individual trees' neighbourhoods, and show via simulated examples how the new indices greatly improve detection of local diversity. We also compare data from Panama and Finland at a shared ecological scale. We conclude that a tree-level data should not be aggregated to any technical scale before computing indicators. The separation of scales also helps produce indicator maps comparable across different studies. We recommend conditional indicators of local diversity over unconditional ones.

1. Introduction

Global biodiversity hotspots are defined as regions with more than 1500 different species and less than 30% of the primary habitat area remaining (Marchese, 2015), and include areas such as the Amazon rainforest and Madagascar. At the national level, biodiversity hotspots would be regions with high conservation value. These hotspots could include e.g. the remaining primeval forests or forest stands (Sabatini et al., 2018). At a more local scale, biodiversity hotspots would be small areas within a landscape or a single stands having higher biodiversity than the surrounding area. By landscape we mean here an area including multiple stands or forest estates (or woodlots). Such local hotspots are of interest e.g. when areas to be conserved are selected (Mikkonen et al., 2023). The identification of local hotspots is also of interest when selecting set-aside areas within a forest estate or within an area to be harvested. This aims at preserving biodiversity in commercial forests through demarcating set-aside areas required in the certification or through preserving groups of rare tree species or trees from previous generations when the area is harvested, and when the tracks within each stand for the harvesting and transportation machinery are planned before the harvest takes place.

The indicators of primeval forests, as an example, include species diversity, the size variation of the trees, and a non-regular spatial pattern of the trees (Myllymäki et al., 2023). To identify primeval forests we therefore want to be able to locally detect areas where either the species composition, size distribution or spatial pattern have a higher variability than the surrounding areas.

Similarly, the indicators of biodiversity that have been used include forest structural and compositional indices such as the Gini–Simpson index for species richness (Tuomisto, 2012), Gini index for size distribution (Valbuena et al., 2016) or Fisher index for spatial pattern (Halme and Mõttus, 2023). Most often these diversity indicators are calculated at systematically or randomly selected locations in the landscape. We advocate as a better alternative the so called "plant's eye view", where the index is conditioned to measure what happens at the data's finest scale, in an individual tree's neighbourhood (Shimatani, 2001; Law et al., 2009; Rajala and Illian, 2012). In point pattern statistics literature, the conditional summaries are traditionally studied as domain

* Corresponding author.
E-mail address: tuomas.rajala@luke.fi (T. Rajala).

https://doi.org/10.1016/j.ecolind.2025.114046
Received 27 January 2025; Received in revised form 8 August 2025; Accepted 12 August 2025

averages, but, in this work, we are interested in mapping, so we define new, localised indices to capture local variation. Our hypothesis is that when we calculate the indicators locally and conditionally, local diversity hot/coldspots can be detected more accurately.

Quantifying biodiversity indicators in the field is time consuming, especially in the tropics (Fricker et al., 2015). Therefore, particularly at large areas, quantification must largely rely on remote sensing data and model-based predictions. In the remote sensing context, the scale of the analysis is typically fixed to the spatial resolution of the used remote sensing material (Fassnacht et al., 2022). Moreover, the predictions include much uncertainty, especially when the data used are satellite image data (Rocchini et al., 2016).

The fixed scale is, however, problematic, as the ecological meaning of local diversity indices varies as a function of the measurement scale (Chisholm et al., 2013; McGlinn et al., 2018). This means that studies with different measurement scale are not necessarily comparable, but can produce contradictory results. Also, spatial scale is an important part of the definition of any diversity metric (Sreekar et al., 2018; O'Shaughnessy et al., 2023). Moreover, ideally the diversity should be presented in multiple scales to understand the phenomenon adequately. Yet, most studies are using just a single scale (Suárez-Castro et al., 2022).

At the highest resolution, single-tree level datasets have usually been small due to field collection costs. However, today's remote sensing technology allows single tree detection and efficient formation of a tree pattern of interest as an output for large areas (Stereńczak et al., 2020; Kostensalo et al., 2023). Remote sensing based tree patterns can have issues, e.g. missing small trees, but solutions are being developed, e.g. for imputing small trees (Kostensalo et al., 2024). We believe that the production and analysis of such large data becomes common in the near future, and in these large tree patterns the desired scales for estimating the diversity itself and the presentation of the (raster) map can be selected independently.

Throughout this work we will emphasise the distinction between two concepts of spatial scale relevant to the production of forest structural and compositional diversity maps: The study scale, and the technical, or presentation, scale. The resolution of the used material, such as satellite images, dictates the smallest possible grain level, and studies using different sources with different spatial resolutions can be incomparable (Fassnacht et al., 2022). When data is available at a single-tree level the study scale and technical scale can be separated, and we will demonstrate the benefits of doing so.

For purposes of this work, by study scale we mean the spatial scale parameter in the definition of a diversity index. This scale parameter defines at which spatial scale (or scales) an ecological process is studied. The archetypal example is the distance parameter $r > 0$, in meters, determining the radius to look around a spatial location. The parameter usually defines what is meant by "in the neighbourhood" or "around here".

In contrast, by technical scale we mean the spatial scale of the final presentation of a diversity index over the spatial domain of interest. Usually this is given by the grid-resolution of a digital raster, say pixel-width $\delta > 0$, in meters, but it can be some other unit of aggregation. The technical scale does not need to be constant over the domain, for example when aggregating to irregularly shaped administration regions. However, if operating with the technical scale only, the map is better studied at coarser scales, because technical scale is bounded below by the data density: Empty cells on too fine a resolution lead to noisy maps.

As a first illustration of the distinction between the two scale concepts, we computed the Gini–Simpson diversity indices (discussed later in Section 3) for two datasets, boreal Evo and tropical BCI (introduced briefly in Section 6). We computed diversity maps using technical scales $\delta = 2^0, \dots, 2^8$ m using what we call the aggregate first-approach, where the index is calculated independently for each raster-cell subset. This traditional approach provides a benchmark in which the study and technical scales are coupled. Then we computed two alternative local maps we developed using a fixed local neighbourhood scale $r = 10$ m and then interpolating to the δ-raster (topic of Section 3). For this illustration we took the mean across each map to represent average local diversity.

The different indices were then plotted to show their dependency on the technical scale (Fig. 1). The average aggregate first-based diversity index is clearly a function of the technical scale (the δ parameter), starting from very low diversity at short scales (as many small cells are empty or with only a single tree), and then converges to the domain diversity as cell size increases (Fig. 1, orange lines). In contrast, when we define local diversity with an explicit study scale (the r parameter), the average diversity across the map remains nearly independent of the technical scale (Fig. 1, blue and green lines correspond to two example indices to be discussed in more detail in Section 3). The average local diversity does not converge to the full domain index, indicating that the diversity at the domain level does not represent the diversity in an average local neighbourhood.

In this work, we have two main objectives. First, we will demonstrate how the study and the technical scale can be separated and how the separation affects the interpretation of the resulting maps. This separation used to be possible only in small, field-measured areas (< 1 km^2), but, using modern remote sensing single-tree detection methods, it is now also possible in large areas (> 1000 km^2). Second, we will show the difference between conditioned and unconditioned indices of tree species diversity, size distribution, and spatial pattern by developing suitable indices and then applying them to simulated data. The field of spatial point pattern statistics studies such conditioning, and we hope that our application of the methodology helps the understanding reach a larger audience. We will also compare two real data sets using the new indices, and, finally, we discuss the reasons why conditional indicators are more recommendable.

2. Materials and methods framework

We consider the setting in which the full data describe the tree locations in some landscape or region of interest. Assume that the region of interest can be represented as a spatial domain $D \subseteq \mathbb{R}^2$. We write $\mathbf{x} = \{[x_i; m_i] : i = 1, \dots, n\}$ for the unordered set of data points, each given as a pair of elements with $x_i \in D$ denoting the point (tree) location and $m_i \in \otimes_{p=1}^{P} M_p$ denoting additional information about that particular tree $i = 1, \dots, n$. The information is often called the tree's mark, and can encode such details as its species, so that $M_p = \{1, \dots, R\}$ where R is the species richness, or diameter-at-breast-height (dbh), so that $M_p = (0, \infty)$. In practice, the data are typically stored in a rectangular data frame (or matrix) with points as rows and coordinates and mark-values as columns.

For mapping variation *locally* within the domain we need to specify what *locally* means. We equate locality to a spatial neighbourhood: For any location in the domain $s \in D$, consider *a neighbourhood* of s to be given by the disc of some fixed radius $r > 0$, denoted by $b(s, r) := \{x \in D : \|x - s\| \leq r\}$. Denote the count of each species-wise pattern $\mathbf{x}_k, k = 1, \dots, R$ by n_k, the local counts by $n_k(s) = n_k(s; r) := \#\{\mathbf{x}_k \cap b(s, r)\}$ and the total number of neighbours by $n(s) = \sum_{k=1}^{R} n_k(s)$.

To draw diversity maps most often raster graphics are used. A raster represents values on a regular grid over the domain. Define a grid as a set of cells $G = \{C_j\}$, with full coverage $D \subseteq \cup_{j=1}^{T} C_j$ and no overlaps $C_i \cap C_j = \emptyset, i \neq j$. Let the points $\{c_j\}$ stand for the cell centroids, and attach some value y_j to each cell. The raster is then the combination $\{[C_j; y_j]\}$. A map is the visual representation of the raster, usually mapping the y_j's to some colour-scale and filling each cell accordingly. We consider regular grids, and let the *resolution* of the grid be δ, i.e. the cells are c_j-centered squares with sidelengths δ, specifically $C_j = c_j + [-\delta/2, \delta/2]^2$.

As the data $\mathbf{x}$ is a point pattern, a convenient analysis framework is given by the theory of spatial point processes (e.g. Illian et al., 2008;

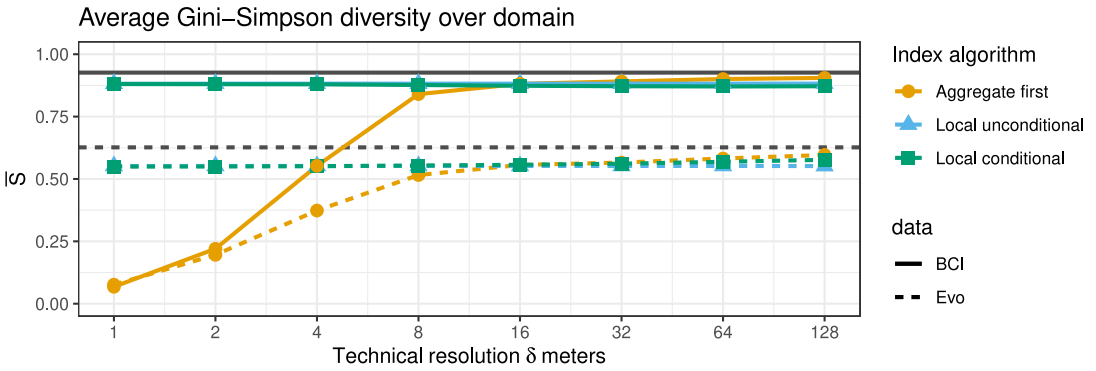

Fig. 1. Effect of technical resolution on the average Gini–Simpson diversity across the map. The non-local indices are presented as black horizontal lines. Local neighbourhood scale $r = 10$ m. Local index map interpolation with Gaussian kernel and $\sigma = \delta/2$.

Baddeley et al., 2015). In this framework, the data $\mathbf{x}$ is modelled to be generated by some spatial or spatio-temporal point process $\mathcal{X}$. In a typical map drawing scenario we have only one snapshot observation $\mathbf{x}$ from $\mathcal{X}$, yet we want to understand its properties, such as local mixing of different species i.e. species diversity.

It might be tempting to start a non-parametric analysis, such as estimating a local diversity index, the classical way, on assumptions of low-order stationarity of $\mathcal{X}$ (e.g. Illian et al., 2008). Roughly put, assumptions of first and second order stationarity of the process $\mathcal{X}$ imply that "means" and "correlations" of the process, respectively, are statistically identical across the domain. These assumptions are in smaller domains justified, and then only spatial averages are relevant. Such assumptions are however not useful for mapping purposes, where we, implicitly or not, do not expect indices to be (statistically) constant and in fact we explicitly want to assess the variations within the domain.

We therefore make no stationarity assumptions. Estimating local variations in point process properties is an ongoing topic, particularly in the estimation of the intensities (points-per-area) (e.g. Diggle, 1985; Cronie and Van Lieshout, 2018), second-order "correlations" (e.g. Getis and Franklin, 2010; D'Angelo et al., 2023), and localised likelihood-based inference for point process models (Baddeley, 2017).

3. Species diversity maps: Evenness of abundances

Any measure of forest diversity will necessarily face the impossibility of satisfactorily capturing a complex system in a few numbers. A typical diversity index summarises the observed species abundances distribution as a one dimensional characteristic, and many such indices in use are closely related. Tuomisto (2012) discusses many such indices, and, emphasising that diversity, evenness and richness are different concepts and measure different things, shows how several of the popular indices are directly related to the three quantities. To be concrete here, consider the distribution of species amongst the trees to be given by frequencies $p = (p_1, \dots, p_R)$, $\sum_{k=1}^R p_k = 1$ where the number of species, R, equals richness. Concentration of this distribution can be seen as a diversity characteristic: Less concentrated distribution means more species are abundant. The uniformity index introduced by Simpson (1949) is a simple way to measure concentration. Most applications use the one-complement of the concentration and measure evenness instead, adopted here as

$$S = 1 - \sum_{k=1}^{R} p_k^2.$$

In this text we call this evenness metric the *Gini–Simpson index* (Tuomisto, 2012). Tuomisto shows that it can be expressed as $S = 1 - 1/{}^2D$ where ${}^2D$ is order 2 version of a more general diversity metric. The index gets a maximum value $(R-1)/R$ when all frequencies are equal, and a minimum value of 0 when one species dominates, i.e. one of the frequencies is one and all others are zero.

With the observed counts of different species in the data, n_k with $n = \sum_{k=1}^R n_k = \#\{\mathbf{x}\}$, an unbiased estimate of the Gini–Simpson index can be computed using

$$\hat{S} = \hat{S}(D) = 1 - \sum_{k=1}^{R} \frac{n_k(n_k-1)}{n(n-1)}.$$

The inclusion of D highlights that $S(D)$ describes the diversity across the whole domain D.

There are now two ways to consider the Gini–Simpson index locally. The first local version, entitled here *unconditional local Gini–Simpson index*, is a straightforward restriction of Gini–Simpson index to local neighbourhoods (cf. Section 2): At some spatial location $s \in D$, define

$$\hat{S}(s) = \hat{S}(b(s,r)) = 1 - \sum_{k=1}^{R} \frac{n_k(s)[n_k(s)-1]}{n(s)[n(s)-1]},$$

where the number of points of species k in $b(s,r)$ is denoted by $n_k(s)$, and $n(s) = \sum_{k=1}^R n_k(s)$. In practice, we compute the index at a fine grid of locations s.

To fully utilise the tree-level point pattern data, the second local version assumes that a tree is at s. Note first that the Gini–Simpson index S can in general be interpreted as the probability of two randomly sampled units from the target population having a different label. The local index $S(s)$ restricts the population to the neighbourhood of the spatial location s. But with point pattern data we can ask a more nuanced question: Given there is a tree at s, what is the probability that one of its neighbours is of a different species? Assuming the location $s = x_i$ is at data point $[x_i, m_i]$ where m_i is its type, we propose to compute the *conditional local Gini–Simpson index* as

$$\tilde{S}([x_i, m_i]; r) = \frac{\sum_{j=1, j\neq i}^{n} 1\big(\|x_i - x_j\| < r\big) 1\big(m_i \neq m_j\big)}{\sum_{j=1, j\neq i}^{n} 1\big(\|x_i - x_j\| < r\big)}.$$

Note that even though $\tilde{S}$ is inspired by the $\alpha(r)$ index discussed by Shimatani (2001), averaging $\tilde{S}$ over points is not Shimatani's estimate $\hat{\alpha}$ because $\hat{\alpha}$ is based on the ratio of domain-averaged Ripley's K-function estimates, which is not the same as the average of ratios of pointwise K-functions. Note also that the conditional local index is undefined if the target point has no neighbours.

In comparison to the two local indices above, recall that we often use a raster to visualise the map. When the raster grid is fixed, say cells $\{C_j\}$, we can divide the point pattern into cell-wise subsets $\mathbf{x}_j = \mathbf{x} \cap C_j$, and then compute the unconditional local Gini–Simpson index each cell independently, $S(C_j)$. This *aggregate first*-approach might seem like an appropriate way to estimate local diversity, but it has two major downsides. First, the grid cells need to be large enough to contain data points for estimation. Second, the grid-resolution and the scale-of-study are necessarily equal, as we discussed in Section 1.

For creating the final map for display we need a colour-mappable value y_j for each grid cell C_j with central location c_j. The aggregate first-approach provides them directly (and fixes the grid), but for the local-versions we need to do some kind of interpolation. We suggest smooth interpolation, e.g. kernel "blurring" by setting $y_j = \sum_{l=1}^{m} S'_l w(\|z_l - c_j\|; \sigma)$ where the sum goes through elements z being either chosen locations s or the data x, the S' is either the unconditional $\hat{S}$ or the conditional $\tilde{S}$, and the w is a kernel function (e.g. Gaussian density) with σ its smoothness parameter.

After displaying the smoothed (or aggregated) map, we look for interesting regions. To highlight statistically interesting regions, we can do a null model test. The diversity, as defined here by the Gini–Simpson evenness index, is conditional on the location pattern, so the null we can test against is the random labelling hypothesis (Illian et al., 2008; Myllymäki et al., 2015). Conditional on the location pattern, the counts in each neighbourhood $n(s)$ are fixed, and we can compare the index value against the null model. Under this hypothesis, the local diversity should follow the domain diversity, so we can compare the observed index, say S^o at s, where S^o is either the observed unconditional $\hat{S}$ or the observed conditional $\tilde{S}$, to a set of values $\{\hat{S}^b(s) : b = 1, \dots, B\}$, where each $\hat{S}^b$ is computed from a randomly sampled species vector $n^b \sim \text{Multinomial}(n(s); p)$. p are again the observed species frequencies. If the rank of S^o compared to $\{\hat{S}^b\}$ is extreme (near 1 or B), we can flag the location s interesting. To bootstrap simultaneously over several scales $r_1, \dots, r_m$, we first center each vector-valued index with the bootstrap average vector $[\bar{S}^{(B)}(r_1), \dots, \bar{S}^{(B)}(r_m)]$, and then choose the component with the highest absolute value, keeping its sign, as a test statistic to rank. For increasing $r_1 < \cdots < r_m$, we sample each vector-valued bootstrap sample $n^b(r_1), \dots, n^b(r_m)$ using the fact that the species vector components in the neighbourhood increments $b(s, r_l) \setminus b(s, r_{l-1})$ are independent under the null. Having established the ranks at point locations (either s or x), we then interpolate them to the output grid. We used the R function `markmean` from the R package `spatstat` (Baddeley et al., 2015) for interpolation, and after some testing found that geometric averaging of ranks works well for hotspot detection.

We will now illustrate the differences between the aggregate first-approach and the two interpolated local neighbourhood approaches to mapping Gini–Simpson diversity. We simulated three point patterns to represent three types of forests, and then combined them side-by-side to form one large, diverse pattern. The resulting point pattern has 3 species with abundances $n \approx (860, 870, 440)$. The domain Gini–Simpson index is 0.64, but the diversity varies locally. We entitled the three different forest sections Segregated, Neutral and Mingling, with a corresponding local effect between the species.[1] The local segregation/mingling should be quantifiable by a diversity metric. We computed the aggregate first-index and the two neighbourhood-based indices for each pattern and measured each unit's (grid cell, spatial location, or tree location) deviation from the mean using the earlier described bootstrap procedure. We combined in the test simultaneously ecological scales 5, 10 and 15 m. For the map the index values and the bootstrap-rank were interpolated to a fine grid, and the rank-map was thresholded at a 5% level.

To summarise the results we visualised the point pattern, the computed diversity maps, and the cold and/or hotspots detected using the bootstrapping procedure (Fig. 2). All approaches, aggregate first, local unconditional and local conditional, are able to correctly detect segregation across the western, segregated region (Fig. 2, left side). The diversity values are clearly lower than the domain average, and the bootstrapping detection highlights many parts of the region. In the neutral region (center) the aggregate first-approach indicates falsely a high proportion (15%) of locations non-neutral, whereas the truly local versions have almost no false positives. In the mingled section the aggregate first-approach detects some cells as super-diverse, but as the rate is similar to the false positive rate of the neutral section these results are unreliable (Fig. 2, right side). More interestingly, the presence of higher-than-expected local diversity is detected clearly with the local conditional index. This is interesting especially when we notice that no significant deviations from neutrality are detected using the local unconditional index.

4. Size diversity maps: Gini index

In addition to species diversity, we can also produce maps of local size diversity. Increased heterogeneity in individual trees' sizes can be interpreted as an indication of higher biodiversity (Gao et al., 2015; Zhang et al., 2024). *The Gini index* G is a popular measure of uniformity of individuals' features (originally income) in a target population. It can be written as the ratio of the mean absolute deviation to the mean, is similar to the coefficient of variation, and higher values indicate larger diversity amongst the values.

Consider mapping the Gini index of tree's dbh, say y_i, across the landscape D. Analogous to the derivation of the local species diversity in Section 3, consider first the full-data index. The commonly used estimator for the Gini index is

$$\hat{G} = \hat{G}(D) = \frac{\frac{1}{n^2} \sum_{i,j=1}^{n} |y_i - y_j|}{2\bar{y}}.$$

We can then consider the *local Gini index* for any subset $A \subseteq D$

$$\hat{G}(A) = \frac{\frac{1}{n^2(A)} \sum_{i,j=1}^{n} |y_i - y_j| 1_A(x_i) 1_A(x_j)}{2\bar{y}_A}$$

with $n(A) = \sum_{i=1}^{n} 1_A(x_i)$ and $\bar{y}_A = \sum_{i=1}^{n} 1_A(x_i) y_i / n(A)$. Here $1_A(x)$ is 1 if data point lies in A, and 0 otherwise.

Given a raster with cells $\{C_j; c_j\}$ we would then compute the map $\{G(C_j)\}$. But again, the interpretation of this map is entirely dependent on the technical resolution. To decouple the technical scale from the study scale, choose a fixed, ecologically interesting scale $r > 0$ and compute $\hat{G}(s) = \hat{G}(b(s, r))$ where s is some spatial location. We call this the *unconditional local Gini* index.

The third and final version we consider is the *conditional local Gini* index: For a tree at x_i of dbh-size y_i let

$$\tilde{G}([x_i; y_i]; r) = \frac{\sum_{j=1, j \neq i}^{n} 1(\|x_i - x_j\| < r) |y_i - y_j|}{2\bar{y}_{b(x_i, r)}}$$

To highlight statistically interesting regions of size diversity, we can use the bootstrap procedure described earlier in Section 3 with the random labelling hypothesis also for $\hat{G}$ and $\tilde{G}$. Under this hypothesis, the sizes should follow the domain size diversity, so the randomly sampled size vector can be drawn from the domain size distribution.

For illustration we again ad-hoc simulated three point patterns to represent three types of diversity and combined them into one large pattern. The resulting point pattern has domain Gini-dbh index 0.28, but the diversity varies locally, depending on the section of the joined pattern. We entitled the three different forest sections under-diverse, neutral and super-diverse, with a corresponding local mixing of dbh's.[2]

[1] We sampled the locations from three separate multivariate Geyer's saturation processes to create a pattern with species-segregation with expected low local diversity, a pattern with no interactions and thus no local diversity structure, and a pattern with species-mingling with expected high local diversity. The patterns were combined with some overlap, and the overlap thinned to keep a constant intensity.

[2] The locations of the under-diverse section where sampled from a Strauss process with strong repulsion up to 3 m and then geostatistically marked with a smooth random field. The neutral section was created from the under-diverse by randomly shuffling the marks. The super-diverse was generated by simulating a mingling 5-type pattern and then giving the classes clearly separated mark $10, 20, \dots, 50$, adding some individual level noise (Gaussian with sd = 2). The marks were then scaled so that when exponentiated to dbh-values, the dbh-values had mean 100 and sd 53. Sections' Gini-dbh indices were .29, .28 and .27.

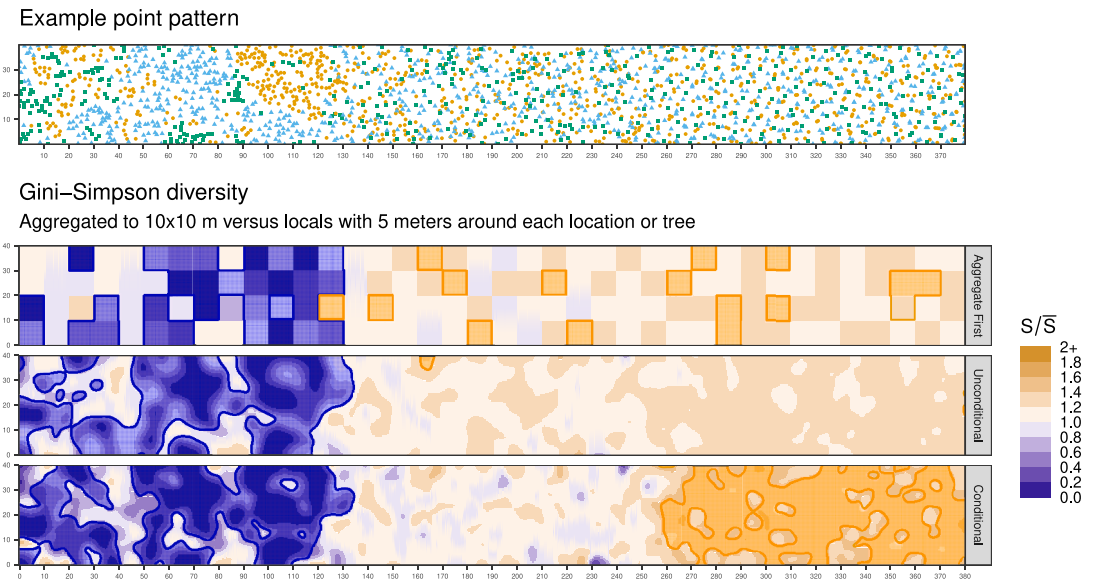

Fig. 2. Comparison of local Gini–Simpson diversity maps on a simulated point pattern, with $n \approx (860, 870, 440)$ and domain Gini–Simpson diversity 0.64. *Top section*: The pattern, exhibiting species segregation (west), neutrality (center) and species mingling (east). *Bottom section*: Gini–Simpson diversity estimated either by aggregate first-approach (top), locally unconditionally (middle) and locally conditionally (bottom). Statistically deviating regions emphasised, tested over scales 5, 10 and 15 m. Index scaled by the per-map mean index.

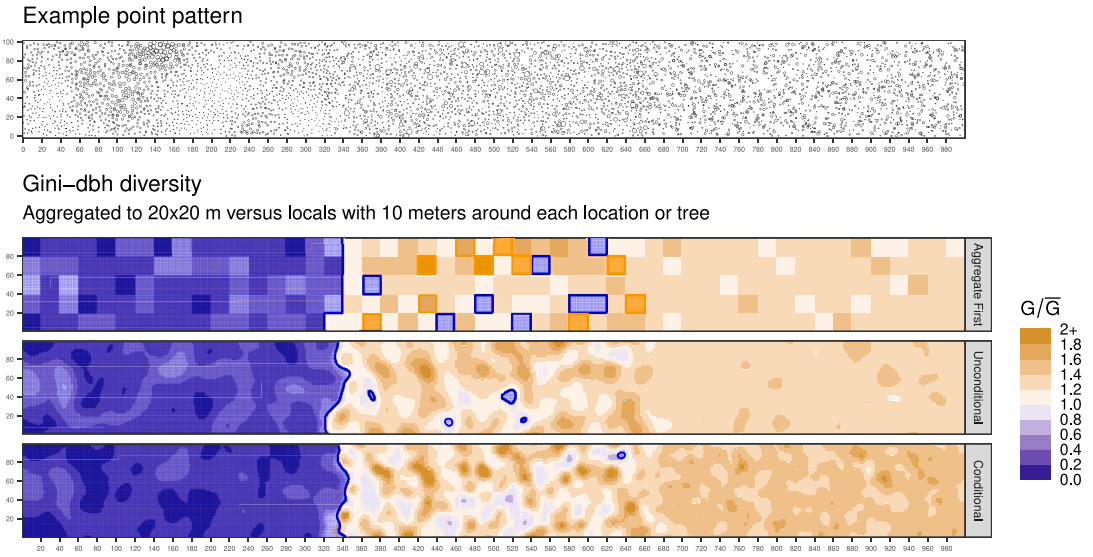

Fig. 3. Comparison of versions of Gini-index of dbh values ("Gini-dbh") using simulated data. The domain Gini-index 0.28. *Top section:* The pattern, exhibiting under-diversity (west), neutrality (center) and super-diversity (east). Drawn size related to dbh. *Bottom section*: Gini-dbh diversity estimated either by aggregate first-approach (top), locally unconditionally (middle) and locally conditionally (bottom). Statistically deviating regions emphasised, tested over scales 5, 10 and 15 m. Index scaled by the per-map mean index ($\bar{G}$).

To summarise the results, we plotted the pattern and the Gini-dbh index maps computed in the three discussed ways (Fig. 3). It is clear that the locally low variability in the under-diverse, western section is well detected by all index versions (Fig. 3, left side). The neutrally mixed region (center) is problematic for the aggregate-first approach which shows a moderate false discovery rate. No index indicates significant hotspots in the eastern, super-diverse section, even though all three suggest some level of positive diversity, with the conditional index being most sensitive.

5. Structural diversity maps: Clustering of locations

Of the list of viewpoints to diversity discussed by Shimatani and Kubota (2004), we have considered species diversity and size diversity. The third diversity viewpoint is related to the complexity of the tree location structure. Such structure is commonly studied as deviations from complete spatial randomness (CSR), and many statistical indices for detecting deviations from CSR are available (see e.g. Illian et al., 2008).

A typical spatial structure index is a *functional* of point pattern data that summarise spatial structure as a function of spatial scale $r > 0$. Well known examples are the Ripley's K-function, describing the average number of neighbours around a tree, and the distribution of distances to nearest neighbours. These summaries are usually averaged over the region and presented as functions of the scale r, approach also taken by Shimatani and Kubota (2004) for all the diversity viewpoints.

To build a raster map of the spatial diversity, we start by recalling the local *product densities*, first discussed by Cressie and Collins (2001)

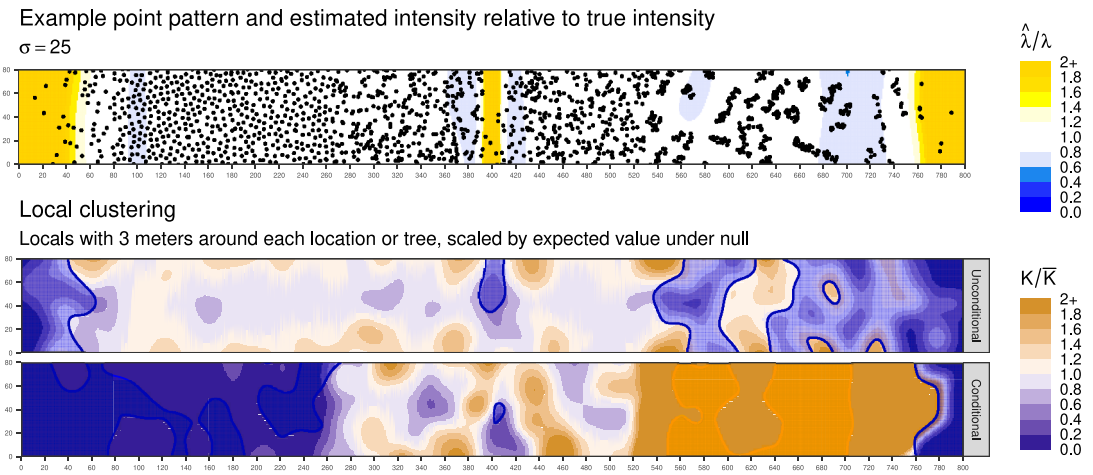

Fig. 4. Comparison of unconditional and conditional clustering diversity using a simulated pattern consisting of a mixture of anti-clustering, complete randomness and clustering and tapered intensity near horizontal edges. *1st section from the top*: The pattern, overlaid on the ratio between the estimated intensity function $\hat{\lambda}$ and the true intensity function λ used in the simulation. *2nd section*: Unconditional and conditional local clustering indices, with the interesting regions highlighted. Interesting regions tested over ranges 1, 3 and 5 m.

and later in their more usual, intensity-scaled form by D'Angelo et al. (2023). The intensity-scaled product density, commonly known as the pair correlation function or radial distribution function, describes the pattern's tendency to be clustered or anti-clustered at a given spatial scale r (Sect. 4.3. Illian et al., 2008). Estimation of product densities involves kernel-smoothing, and such estimates are always biased and can be sometimes sensitive to the chosen kernel parameters. Furthermore, without stationarity assumptions, like in our large region mapping task, the use of the inhomogeneous versions of pair correlation and the K-function is tricky, even at the full data level: Accurate intensity-scaling requires the knowledge of the local intensity, but it is in practice notoriously difficult to estimate well.

Keeping these pitfalls in mind, we now define a version of the local K-function to study spatial structure. In our notation, the number of data points in a set $A \subseteq D$ is written as $n(A)$. Following the logic of Section 3, we can compute the number of points either conditionally or unconditionally. We define the *unconditional clustering index* K_u at s as

$$K_u(s) = \hat{\lambda}(s)^{-1} \sum_{i=1}^{n} 1\big(\|x_i - s\| < r\big) = \frac{\sum_{i=1}^{n} 1\big(\|x_i - s\| < r\big)}{c_\sigma \sum_{i=1}^{n} w\big(\|x_i - s\|; \sigma\big)}$$

where $\hat{\lambda}$ is an estimate of the local intensity, and a typical form for a kernel density estimator of it is shown in the denominator on the right (c_σ is a normalising constant). The *conditional clustering index* K_c at x we compute as

$$\begin{aligned} K_c(x) &= \hat{\lambda}(x)^{-1} \sum_{i=1}^{n} 1\big(\|x_i - x\| < r\big) 1\big(x \neq x_i\big) \\ &= \frac{\sum_{i=1}^{n} 1\big(\|x_i - x\| < r\big) 1\big(x_i \neq x\big)}{c_\sigma \sum_{i=1}^{n} w\big(\|x_i - x\|; \sigma\big)}. \end{aligned}$$

The difference is that in the conditional version we are not counting the point itself. This difference might seem irrelevant, but remember we compute the conditional statistic only at the datapoints. This way we measure between-datapoint clustering, whereas the unconditional index measures clustering of datapoints in relation to landscape (space) instead.

In other words, the unconditional index is similar to the intensity estimator (with a boxcar kernel), and measures how much the intensity varies at scale r when compared to the intensity $\hat{\lambda}$ estimated at scale (roughly) 2σ. The conditional, K-function-type index is instead a second order characteristic: It measures the amount of further points around a point, and contrasts that, up to proportionality constant, to what one might expect with the intensity around there. First order clustering and inhomogeneity are hard to differentiate, as it all depends on the scales used in K_c, K_u and $\hat{\lambda}$: For example, if the scales are equal, K_u is roughly constant across the landscape. Second order correlation is also connected to first order clustering, and since in most cases we do not (and often, cannot) have replicated observations of the process, the difficulty in estimating the local second order correlation boils down to difficulties in correctly estimating and subsequently removing the first order clustering effect from the second order index.

The problem of estimating a non-constant intensity relates to the problem of general density estimation, and many nonparametric and parametric methods exist (see discussions in van Lieshout, 2012; Waagepetersen and Guan, 2009; Baddeley, 2017). For the purposes of this discussion we ignore modelling and tesselation-methods and apply kernel smoothing, as it is relatively cheap to compute and easy to parametrise. A fixed smoothing bandwidth corresponds to an assumption that the intensity is approximately locally constant and does not change too rapidly. Obvious problems arise at locations near roads, forest patch edges, and other such interfaces. For a large domain with many such features it can be beneficial to consider adaptive forms of smoothing (e.g. Baddeley et al., 2022).

With these caveats in mind, we demonstrate the differences between the conditional and unconditional local K-functions using a Gaussian-kernel estimated intensity with a fixed smoothing parameter σ = 10 m. The simulated example data exhibits a mixture of anti-clustering, complete spatial randomness, and clustering, with reduced intensity (1) near west and east ends of the region and (2) on a narrow vertical strip in the center of the region. When checking for interesting regions, we do not bootstrap with fixed data locations, in particular fixed neighbour counts, like in Sections 3 and 4. We instead bootstrap the neighbour counts (the numerators) using the CSR null model hypothesis, particularly the fact that under null the neighbour count around a location x, regardless of there being a tree or not, is Poisson distributed with intensity $\int_{b(x,r)} \lambda(s) ds$.

We show the point pattern overlaid on the relative bias in the intensity estimate that was used to adjust for first-order clustering, together with the computed unconditional and conditional indices (Fig. 4). We can immediately see that unconditional and the conditional maps are very different (Fig. 4, rows 2 and 3). The unconditional index interprets large empty areas between tight clusters in the east as anti-clustering, and the strong anti-clustering in the west goes unnoticed (Fig. 4, left and right ends). The conditional index clearly indicates the second-order anti-clustering and clustering regions. False detections

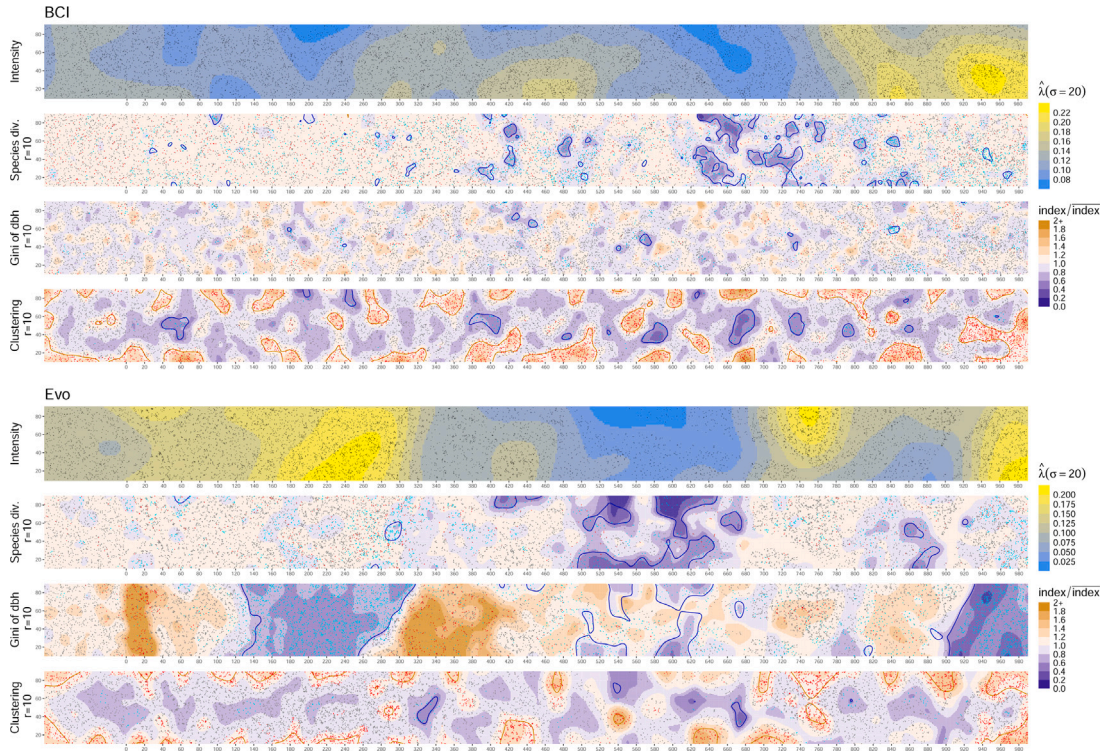

Fig. 5. Diversity maps for the BCI and Evo data 1000 × 100 m subsets. From the top: Estimated intensity; Gini–Simpson species diversity; Gini-index of dbh; Local clustering index. Local indices visualised at local scale $r = 10$ m. Tree locations overlaid with dots. Significant deviations estimated over $r = 5, 10, 15$ m and highlighted per point by cyan/red colour for low/high deviation, and spatially by dark contour-lines. Leftmost 100 × 100 m area contains a purely randomly generated pattern to check against false positives.

arise near the west and east ends and the center of the region, where the true intensities drop. The kernel intensity estimate is over-estimated with the chosen bandwidth, leading to relatively high denominators in the index formulas, and therefore low index values, so these regions get interpreted as anti-clustered (Fig. 4, top row, yellow colour).

6. Real data example: Boreal and tropical forest diversities compared

As a final illustration we computed the various diversity maps for two forest datasets. Barro Colorado Island (BCI) dataset is part of a long term rainforest study plot on Barro Colorado Island in Panama (Condit et al., 2019). Every woody plant with stem diameter at breast height larger than 1 cm was recorded in a 1000 × 500 m region. We analyse from the 2010 census the location pattern of all living main-stems of known tree species in a 1000 × 100 m subset by the northern edge. In this subset $n \approx 14000$, species count is 84, Gini–Simpson is 0.92 and Gini of dbh is 0.30. This data is used to demonstrate the effect of higher variability to the detection of local hot/coldspots.

The second dataset is a computed forest treemap from Evo region in Finland Kostensalo et al. (2024), constructed using airborne laser scanning techniques and augmented with stochastic imputation of small trees based on data from field plots (Kostensalo et al., 2023). We analyse all tree stems in a 1000 × 100 m subarea near central Evo, with $n \approx 12500$. We consider pine, spruce and deciduous (grouped) stems so species count is 3, with Gini–Simpson 0.63 and Gini of dbh 0.32. This data is used to illustrate the potential of remote-sensing based single-tree detection in detecting the local hot/coldspots.

For both datasets we add to western edge an extra 100 × 100 m section with homogeneous, purely random data matching the average tree density and the dbh and species distributions. The purpose of this test region is to gauge the amount of false positives that might appear in the maps. For both sets the scale of stem intensity is similar so we set the local scale of study at $r = 10$ m, and test for deviations from null using scales 5,10 and 15 m. For the intensity estimation we set the smoothing bandwidth to $\sigma = 20$ m.

We present here only the conditional results of the BCI and Evo diversity maps (Fig. 5). BCI tree local intensity varies from 0.08 to 0.22, Evo more from 0.02 to 0.20 (intensity drops at roads that intersect the Evo region). By studying and contrasting the Gini–Simpson maps, we observe that species diversity is mostly homogeneous in both datasets, but we also observe that both datasets have subareas of low species diversity, and these pockets of low diversity are smaller in BCI than in Evo (Fig. 5, second rows). One possible explanation is that in BCI these pockets are filled with light-gap specialists, and in Evo the gaps are more related to management.

The dbh diversity is fairly homogeneous in BCI, but in Evo there are large sections which are of low diversity, meaning stem sizes are very homogeneous (Fig. 5, third rows). These observations can be explained by BCI being a fairly undisturbed, natural rainforest with a diverse age-structure, whereas Evo has been previously managed.

Against the varying intensity, clustering and anticlustering seems to alternate in small islands through the BCI region, Evo being more homogeneous in spatial diversity with only a few deviations (Fig. 5, fourth rows). Here we hesitate to interpret the map further since by looking at the added test region, the rate of false positives seems to be higher than with the other indices, likely due to issues with the estimated intensities (Fig. 5, westernmost 100 × 100 m). Overall, the forests differ clearly in size diversity, with BCI being more diverse, and spatial diversity, with BCI exhibiting more heterogeneity in clustering/anticlustering structure over the region. While the whole BCI may be regarded as a biodiversity hotspot, and Evo not, studying local diversities within the region like done above provides further details on how the diversity of each forest area varies across the landscape.

7. Discussion

The presented case studies demonstrate that whenever a tree-level point pattern is available as data it should not be aggregated to any technical scale before calculating diversity indicators. Aggregating data to raster cells and then estimating diversity does not provide the same information as first estimating local diversity and then aggregating (averaging). We showed that the sensitivity of the indicators to variations in local diversity suffers from pre-aggregation. Pre-aggregating point location data to cell-level data is tempting because it simplifies e.g. storage and parallel processing, but the scales become convoluted and the chosen cell size effectively sets a lower bound to the desired, scientifically relevant scales. Furthermore, by considering the technical and study scales separate, we are able to produce comparable diversity indicator maps across studies, since a desired scale can always be selected.

Pre-aggregation aside, to fully utilise the tree-level data, we developed new, localised versions of well-known diversity indices. With them, we demonstrated that when diversity indicators are conditioned to summarise the local neighbourhoods exactly at tree locations, we get indicators that are more sensitive to diversity variation than the indicators that summarise neighbourhoods of arbitrary spatial locations. In case of spatial diversity, the discrepancy between the indicator versions is the greatest, as the tree-conditioned version describes point-to-point correlations, while the unconditioned version describes point-to-landscape correlations. The two definitions coincide only under complete randomness of the tree locations, which does not hold e.g. in managed forests. In case of species and size diversity, the unconditional indices seem to be better suited for detecting areas with low diversity, such as patches of singular species or size. Patchiness is a type of first-order property (cf. discussion on clustering and inhomogeneity, Section 5). The conditional indices can detect such under-diversity, too. But as second-order statistics they also detect local super-diversity. To explain this discrepancy one needs to understand that instead of just being sensitive to patchiness in the landscape, a first order property, the conditional indices are sensitive to point-to-point correlations, a second order property: Conditioning on a point fundamentally changes what type of information a point pattern index summarises (see e.g. Illian et al., 2008, p. 177).

We also presented simple tests for the differences between the local indicator values and the larger area mean, which allowed us to check if the differences were statistically significant. Such a simple test could be used e.g. in directing field work in order to check if the detected hotspot is an actual hotspot. Field checking is recommendable, as no single forest structural diversity index alone determines if a location is a biodiversity hotspot.

The simplistic formulas for the presented indices differ from what is common in point pattern statistics. Border bias, which happens under stationarity assumptions when neighbourhoods near the domain border get clipped with the border, was not addressed here because we have no well defined borders and, more importantly, we did not assume spatial stationarity. Constructing domain borders and accounting for them e.g. by adaptive smoothing should improve estimation near those borders, for example near waterways and roads. Adaptive smoothing could also help mitigate biases in intensity estimates, which are likely behind the high false positive rates of the clustering maps (Section 5). There is a trade-off between too little and too much detected clustering as a function of intensity estimate smoothness: Overestimated, i.e. too variable, intensity surface leads to underestimated clustering, and underestimated, i.e. too flat, intensity surface leads to overestimated clustering. The only generally applicable advice we dare to provide here is that when using simple kernel smoothing, check the sensitivity of the clustering maps to different kernel smoothnesses.

For the visualisation of hotspots, we rather naïvely applied existing tools for fast interpolation directly on point-wise bootstrap ranks to smooth the local test results. This is an ad-hoc approach, and we inspected only visually that the rank-smoothing works. The approach should be properly analysed to understand its potential and limitations, and to understand how, for example, it might be linked to the false positives in the spatial clustering analysis (Section 6). We also think that even though the pointwise testing has the highest spatial resolution, it also uses the lowest amount of information and can have low statistical power. Increasing the power at the cost of some smoothing bias could be worth pursuing, perhaps by locally weighted averaging like in the local likelihood approach by Baddeley (2017).

Traditional field data from which local indicators of biodiversity can be estimated are rarely available. However, increasingly higher quality single-tree level remote sensing data are being produced and it is now possible to map large areas (Kostensalo et al., 2023). Single-tree detection is typically carried out only for fairly large trees (Hyyppä et al., 2024). The data including only large trees are not necessarily useful for mapping biodiversity, especially considering the reduced variation in the Gini index and in the spatial clustering. The smallest trees are not visible from airborne laser scanning, but their occurrence can be predicted (Kostensalo et al., 2023, 2024). The fact that they are predicted rather than measured may introduce variation in the locations of the significant hotspots, but it reduces bias due to the non-detection.

The single-tree detection augmented with predicted small trees has been proven to provide realistic tree patterns in boreal conditions. Since the method has not yet been tested in more complex forests, the reliability of the produced tree patterns in these conditions is not known. It can be assumed that single-tree detection without any augmentation for undetected trees works better in boreal conditions than in the temperate or tropical areas. However, the increasing laser scanning point densities and the development of augmentation techniques could markedly reduce the difference in the future (Stereńczak et al., 2020). If this turns out to be correct, the proposed aggregate-late approach could be reliably applied in more complex forests as well.

Calculating the indicators from augmented tree patterns produces promising results (Kostensalo et al., 2023), but the uncertainties involved are not yet well understood. However, we believe that the discussed aggregate-late way is a valid alternative to the more traditional approach of producing indicator maps by using a statistical model to predict directly to raster cells from a sample of field data, an approach with also many uncertainties (Häbel et al., 2021; Ørka et al., 2022).

CRediT authorship contribution statement

Tuomas Rajala: Writing – original draft, Methodology, Investigation, Formal analysis, Conceptualization. **Annika Kangas:** Writing – review & editing, Conceptualization. **Mari Myllymäki:** Writing – review & editing, Methodology, Funding acquisition, Conceptualization.

Declaration of competing interest

The authors declare that they have no known competing financial interests or personal relationships that could have appeared to influence the work reported in this paper.

Acknowledgements

The research was financially supported by the European Union—NextGenerationEU in the Research Council of Finland's project (Grant number 348154) under the Research Council of Finland's flagship ecosystem for Forest-Human–Machine Interplay—Building Resilience, Redefining Value Networks and Enabling Meaningful Experiences (UNITE) (Grant numbers 357909 and 359174). We thank Joel Kostensalo (Luke) for the Evo tree map. The field sampling and sample plot measurements in the Evo data used to

construct the tree map were designed by S. Tuominen (Luke), and acquisition of remote sensing and field data in the Evo region was financed by Finland's Ministry of Agriculture and Forestry/key project "Wood on the move and new products from forests".

Data availability

Data will be made available on request.

References

Baddeley, A., 2017. Local composite likelihood for spatial point processes. Spat. Stat. 22, 261–295. http://dx.doi.org/10.1016/j.spasta.2017.03.001.

Baddeley, A., Davies, T.M., Rakshit, S., Nair, G., McSwiggan, G., 2022. Diffusion Smoothing for Spatial Point Patterns. Stat. Sci. 37 (1), http://dx.doi.org/10.1214/21-STS825.

Baddeley, A., Rubak, E., Turner, R., 2015. Spatial Point Patterns: Methodology and Applications with R. Chapman and Hall/CRC.

Chisholm, R.A., Muller Landau, H.C., Abdul Rahman, K., Bebber, D.P., Bin, Y., Bohlman, S.A., Bourg, N.A., Brinks, J., Bunyavejchewin, S., Butt, N., Cao, H., Cao, M., Cárdenas, D., Chang, L.W., Chiang, J.M., Chuyong, G., Condit, R., Dattaraja, H.S., Davies, S., Duque, A., Fletcher, C., Gunatilleke, N., Gunatilleke, S., Hao, Z., Harrison, R.D., Howe, R., Hsieh, C.F., Hubbell, S.P., Itoh, A., Kenfack, D., Kiratiprayoon, S., Larson, A.J., Lian, J., Lin, D., Liu, H., Lutz, J.A., Ma, K., Malhi, Y., McMahon, S., McShea, W., Meegaskumbura, M., Mohd. Razman, S., Morecroft, M.D., Nytch, C.J., Oliveira, A., Parker, G.G., Pulla, S., Punchi Manage, R., Romero-Saltos, H., Sang, W., Schurman, J., Su, S.H., Sukumar, R., Sun, I.F., Suresh, H.S., Tan, S., Thomas, D., Thomas, S., Thompson, J., Valencia, R., Wolf, A., Yap, S., Ye, W., Yuan, Z., Zimmerman, J.K., 2013. Scale-dependent relationships between tree species richness and ecosystem function in forests. J. Ecol. 101 (5), 1214–1224. http://dx.doi.org/10.1111/1365-2745.12132.

Condit, R., Pérez, R., Aguilar, S., Lao, S., Foster, R., Hubbell, S., 2019. Complete Data from the Barro Colorado 50-Ha Plot: 423617 Trees, 35 Years. Dryad, http://dx.doi.org/10.15146/5XCP-0D46, 573292682 bytes.

Cressie, N., Collins, L.B., 2001. Analysis of spatial point patterns using bundles of product density LISA functions. J. Agric. Biol. Environ. Stat. 6 (1), 118–135. http://dx.doi.org/10.1198/108571101300325292.

Cronie, O., Van Lieshout, M.N.M., 2018. A non-model-based approach to bandwidth selection for kernel estimators of spatial intensity functions. Biometrika 105 (2), 455–462. http://dx.doi.org/10.1093/biomet/asy001.

D'Angelo, N., Adelfio, G., Mateu, J., Cronie, O., 2023. Local Inhomogeneous Weighted Summary Statistics for Marked Point Processes. J. Comput. Graph. Stat. 1–15. http://dx.doi.org/10.1080/10618600.2023.2206441.

Diggle, P., 1985. A Kernel Method for Smoothing Point Process Data. Appl. Stat. 34 (2), 138. http://dx.doi.org/10.2307/2347366, arXiv:2347366.

Fassnacht, F.E., Müllerová, J., Conti, L., Malavasi, M., Schmidtlein, S., 2022. About the link between biodiversity and spectral variation. Appl. Veg. Sci. 25 (1), e12643. http://dx.doi.org/10.1111/avsc.12643.

Fricker, G.A., Wolf, J.A., Saatchi, S.S., Gillespie, T.W., 2015. Predicting spatial variations of tree species richness in tropical forests from high-resolution remote sensing. Ecol. Appl. 25 (7), 1776–1789. http://dx.doi.org/10.1890/14-1593.1.

Gao, T., Nielsen, A.B., Hedblom, M., 2015. Reviewing the strength of evidence of biodiversity indicators for forest ecosystems in europe. Ecol. Indic. 57, 420–434. http://dx.doi.org/10.1016/j.ecolind.2015.05.028, URL: https://www.sciencedirect.com/science/article/pii/S1470160X15002502.

Getis, A., Franklin, J., 2010. Second-Order Neighborhood Analysis of Mapped Point Patterns. In: Anselin, L., Rey, S.J. (Eds.), Perspectives on Spatial Data Analysis. Springer Berlin Heidelberg, Berlin, Heidelberg, pp. 93–100. http://dx.doi.org/10.1007/978-3-642-01976-0_7.

Häbel, H., Balazs, A., Myllymäki, M., 2021. Spatial analysis of airborne laser scanning point clouds for predicting forest structure. Math. Comput. For. Nat. Resour. Sci. 13, 15–28, arXiv:https://www.mcfns.com/index.php/Journal/article/view/13.2/2021.2.

Halme, E., Mõttus, M., 2023. Improved parametrisation of a physically-based forest reflectance model for retrieval of boreal forest structural properties. Silva Fenn. 57, http://dx.doi.org/10.14214/sf.22028.

Hyyppä, M., Turppa, T., Hyyti, H., Yu, X., Handolin, H., Kukko, A., Hyyppä, J., Virtanen, J.-P., 2024. Concepts Towards Nation-Wide Individual Tree Data and Virtual Forests. ISPRS Int. J. Geo-Inform. 13 (12), 424. http://dx.doi.org/10.3390/ijgi13120424, URL: https://www.mdpi.com/2220-9964/13/12/424. Number: 12 Publisher: Multidisciplinary Digital Publishing Institute.

Illian, J., Penttinen, A., Stoyan, H., Stoyan, D., 2008. Statistical Analysis and Modelling of Spatial Point Patterns. John Wiley & Sons.

Kostensalo, J., Mehtätalo, L., Tuominen, S., Packalen, P., Myllymäki, M., 2023. Recreating structurally realistic tree maps with airborne laser scanning and ground measurements. Remote Sens. Environ. 298, 113782. http://dx.doi.org/10.1016/j.rse.2023.113782, URL: https://www.sciencedirect.com/science/article/pii/S0034425723003334.

Kostensalo, J., Packalen, P., Kuronen, M., Mehtätalo, L., Tuominen, S., Myllymäki, M., 2024. Large-Scale Tree-Level Mapping of Forest Structure Including Species with Remote Sensing Data and Ground Measurements. http://dx.doi.org/10.2139/ssrn.4800302, URL: https://papers.ssrn.com/abstract=4800302.

Law, R., Illian, J., Burslem, D.F.R.P., Gratzer, G., Gunatilleke, C.V.S., Gunatilleke, I.a.U.N., 2009. Ecological information from spatial patterns of plants: insights from point process theory. J. Ecol. 97 (4), 616–628. http://dx.doi.org/10.1111/j.1365-2745.2009.01510.x, _eprint:.

Marchese, C., 2015. Biodiversity hotspots: A shortcut for a more complicated concept. Glob. Ecol. Conserv. 3, 297–309. http://dx.doi.org/10.1016/j.gecco.2014.12.008.

McGlinn, D.J., Xiao, X., May, F., Gotelli, N.J., Engel, T., Blowes, S.A., Knight, T.M., Purschke, O., Chase, J.M., McGill, B.J., 2018. Mob (measurement of biodiversity): a method to separate the scale-dependent effects of species abundance distribution, density, and aggregation on diversity change. http://dx.doi.org/10.1101/244103, BioRxiv. arXiv:https://www.biorxiv.org/content/early/2018/08/03/244103.full.pdf, URL: https://www.biorxiv.org/content/early/2018/08/03/244103.

Mikkonen, N., Leikola, N., Lehtomäki, J., Halme, P., Moilanen, A., 2023. National high-resolution conservation prioritisation of boreal forests. Forest Ecol. Manag. 541, 121079. http://dx.doi.org/10.1016/j.foreco.2023.121079, URL: https://www.sciencedirect.com/science/article/pii/S0378112723003134.

Myllymäki, M., Grabarnik, P., Seijo, H., Stoyan, D., 2015. Deviation test construction and power comparison for marked spatial point patterns. Spat. Stat. 11, 19–34. http://dx.doi.org/10.1016/j.spasta.2014.11.004, arXiv:1306.1028.

Myllymäki, M., Tuominen, S., Kuronen, M., Packalen, P., Kangas, A., 2023. The relationship between forest structure and naturalness in the finnish national forest inventory. For.: An Int. J. For. Res. 97 (3), 339–348. http://dx.doi.org/10.1093/forestry/cpad053, arXiv:https://academic.oup.com/forestry/article-pdf/97/3/339/57501343/cpad053.pdf.

Ørka, H.O., Jutras-Perreault, M.-C., sset, E.N., Gobakken, T., 2022. A framework for a forest ecological base map - an example from Norway. Ecol. Indic. 136, 108636. http://dx.doi.org/10.1016/j.ecolind.2022.108636, URL: https://www.sciencedirect.com/science/article/pii/S1470160X22001078.

O'Shaughnessy, K.A., Knights, A.M., Hawkins, S.J., Hanley, M.E., Lunt, P., Thompson, R.C., Firth, L.B., 2023. Metrics matter: Multiple diversity metrics at different spatial scales are needed to understand species diversity in urban environments. Sci. Total Environ. 895, 164958. http://dx.doi.org/10.1016/j.scitotenv.2023.164958.

Rajala, T., Illian, J., 2012. A family of spatial biodiversity measures based on graphs. Environ. Ecol. Stat. 19 (4), 545–572. http://dx.doi.org/10.1007/s10651-012-0200-9.

Rocchini, D., Boyd, D.S., Féret, J.B., Foody, G.M., He, K.S., Lausch, A., Nagendra, H., Wegmann, M., Pettorelli, N., 2016. Satellite remote sensing to monitor species diversity: potential and pitfalls. Remote. Sens. Ecol. Conserv. 2 (1), 25–36. http://dx.doi.org/10.1002/rse2.9.

Sabatini, F.M., Burrascano, S., Keeton, W.S., Levers, C., Lindner, M., Pötzschner, F., Verkerk, P.J., Bauhus, J., Buchwald, E., Chaskovsky, O., Debaive, N., Horváth, F., Garbarino, M., Grigoriadis, N., Lombardi, F., Marques Duarte, I., Meyer, P., Midteng, R., Mikac, S., Mikoláš, M., Motta, R., Mozgeris, G., Nunes, L., Panayotov, M., Ódor, P., Ruete, A., Simovski, B., Stillhard, J., Svoboda, M., Szwagrzyk, J., Tikkanen, O.-P., Volosyanchuk, R., Vrska, T., Zlatanov, T., Kuemmerle, T., 2018. Where are europe's last primary forests? Divers. Distrib. 24 (10), 1426–1439. http://dx.doi.org/10.1111/ddi.12778.

Shimatani, K., 2001. Multivariate point processes and spatial variation of species diversity. Forest Ecol. Manag. 142 (1–3), 215–229. http://dx.doi.org/10.1016/S0378-1127(00)00352-2.

Shimatani, K., Kubota, Y., 2004. Quantitative assessment of multispecies spatial pattern with high species diversity. Ecol. Res. 19 (2), 149–163. http://dx.doi.org/10.1111/j.1440-1703.2003.00619.x.

Simpson, E.H., 1949. Measurement of Diversity. Nature 163 (4148), http://dx.doi.org/10.1038/163688a0, 688–688.

Sreekar, R., Katabuchi, M., Nakamura, A., Corlett, R.T., Slik, J.W.F., Fletcher, C., He, F., Weiblen, G.D., Shen, G., Xu, H., Sun, I.F., Cao, K., Ma, K., Chang, L.-W., Cao, M., Jiang, M., Gunatilleke, I.A.U.N., Ong, P., Yap, S., Gunatilleke, C.V.S., Novotny, V., Brockelman, W.Y., Xiang, W., Mi, X., Li, X., Wang, X., Qiao, X., Li, Y., Tan, S., Condit, R., Harrison, R.D., Koh, L.P., 2018. Spatial scale changes the relationship between beta diversity, species richness and latitude. R. Soc. Open Sci. 5 (9), 181168. http://dx.doi.org/10.1098/rsos.181168.

Stereńczak, K., Kraszewski, B., Mielcarek, M., Piasecka, Ż., Lisiewicz, M., Heurich, M., 2020. Mapping individual trees with airborne laser scanning data in an European lowland forest using a self-calibration algorithm. Int. J. Appl. Earth Obs. 93, 102191. http://dx.doi.org/10.1016/j.jag.2020.102191.

Suárez-Castro, A.F., Raymundo, M., Bimler, M., Mayfield, M.M., 2022. Using multi-scale spatially explicit frameworks to understand the relationship between functional diversity and species richness. Ecography 2022 (6), e05844. http://dx.doi.org/10.1111/ecog.05844.

Tuomisto, H., 2012. An updated consumer's guide to evenness and related indices. Oikos 121 (8), 1203–1218. http://dx.doi.org/10.1111/j.1600-0706.2011.19897.x.

Valbuena, R., Eerikäinen, K., Packalen, P., Maltamo, M., 2016. Gini coefficient predictions from airborne lidar remote sensing display the effect of management intensity on forest structure. Ecol. Indic. 60, 574–585. http://dx.doi.org/10.1016/j.ecolind.2015.08.001, URL: https://www.sciencedirect.com/science/article/pii/S1470160X15004227.

van Lieshout, M.-C.N.M., 2012. On Estimation of the Intensity Function of a Point Process. Methodol. Comput. Appl. 14 (3), 567–578. http://dx.doi.org/10.1007/s11009-011-9244-9.

Waagepetersen, R., Guan, Y., 2009. Two-step estimation for inhomogeneous spatial point processes. J. R. Stat. Soc. B 71 (3), 685–702. http://dx.doi.org/10.1111/j.1467-9868.2008.00702.x.

Zhang, L., Quinn, B.K., Hui, C., Lian, M., Gielis, J., Gao, J., Shi, P., 2024. New indices to balance α-diversity against tree size inequality. J. For. Res. 35 (1), 31. http://dx.doi.org/10.1007/s11676-023-01686-3.